High Density Magnetized Toroid Formation and Translation within XOCOT: An Annular Field Reversed Configuration Plasma Concept

David Kirtley[*], Dr. Alec D. Gallimore[$]

University of Michigan, Ann Arbor, MI 48109

Dr. James Haas[†], Michael Reilly[‡]

Air Force Research Laboratory, Edwards AFB, CA 93524

Abstract

An annular field reversed configuration (FRC) plasma concept is being developed by the Univeristy of Michigan and AFRL to investigate inductively-coupled high power electric propulsion. Presented is the continued exploration of an annular FRC with specific focus on main bank discharges, magnetized plasma toroid formation, and preliminary investigation into plasma translation. Additional detail is given towards discharge parameter space, optimization of energy input/translation, and predictive scaling laws of magnetic flux, plasma density, and plasma energy content. The discharge parameter space covers multiple charging energies, voltages, and timing as well as multiple propellants and pre-ionization techniques. Finally, a case for FRC formation is made by investigating magnetic field (and flux) reversal in the coil as well as downstream magnetic field modification by a high density magnetized plasma.

---

[*]Graduate Student, Aerospace Engineering, dkirtley@umich.edu.

[$] Professor and Laboratory Director, Aerospace Engineering, Associate Dean, Horace H. Rackham School of Graduate Studies, alec.gallimore@umich.edu.

[†] Senior Research Scientist, Group Lead Spacecraft Branch, AFRL/PRSS. james.haas@edwards.af.mil

[‡] Research Scientist, Spacecraft Branch. michael.reilly.ctr@edwards.af.mil

Nomenclature

A	=	Flux collection area for an E/M probe, m^2
Ap	=	Area of cylindrical probe, m^2
β	=	The ratio of magnetic to particle pressures
B_p	=	AFRC magnetic field, measured at the exterior coil surface with plasma, Gauss
B_v	=	AFRC magnetic field, measured at the exterior coil surface without plasma, Gauss
C	=	Capacitance, F/m
e	=	Electron charge
k_b	=	Boltzmann's constant, 1.38×10^{-23} J/K
λD	=	Debye length, cm or mm
I	=	Probe collected current, mA
I_e, I_{sat}	=	Electron saturation current, A
I_{ion}, I_{sat}	=	Ion saturation current, A
M_e	=	Electron mass, 9.1094×10^{-31} kg
M_i	=	Argon Ion mass, 6.69×10^{-26} kg
μ_0	=	Permeability of free space, $4\pi \times 10^{-7}$ $WbA^{-1}T^{-1}$
n_e	=	Plasma electron density, m^{-3}
N	=	Number of turns for an E/M probe
δ	=	Sheath thickness, cm
Φ_ρ	=	Magnetic flux at the annular wall, plasma, Gauss-cm^2
Φ_v	=	Magnetic flux at the annular wall, vacuum, Gauss-cm^2
R	=	Radius of the annular chamber, m or cm
τ	=	Characteristic plasma resonance time, μs
Te	=	Maxwellian plasma electron temperature, eV
V_Δ	=	Double probe applied bias, V
V_{bp}	=	Magnetic probe voltage, relative to diagnostic earth ground , V
V_{bias}	=	Triple Probe applied bias, V
V_c	=	Discharge coil voltage, relative to capacitor return, kV

Introduction

Field reversed theta pinch fusion reactor concepts have been examined in many different laboratories since 1958[1], in a number of configurations: Field Reversed Theta Pinches, Compact Toroid Reactors, and Field Reversed Configuration (FRC) Reactors[1]. These experiments have focused on expanding the confinement times, overall dimensions, energy input, and plasma densities of FRC based concepts. As a fusion concept, benefits included: Larger confinement β, higher densities, and increased stability. In addition, there is extensive literature and over 40 years of developmental research detailing scaling laws and efforts to gain understanding of FRC development and compression processes. Recent developments and concepts have re-energized the field and brought significant interest and study into the physics of FRC formation and translation[2]. Physically, a field reversed configuration plasma is a charge-neutral, dense plasma, which due to the current reversal in the formation pinch (differentiating this from a standard theta-pinch in which there is only a large, positive highspeed current pulse) has completely closed, self-consistent internal magnetic field lines. Plasma that is essentially disconnected from its formation field lines in this way has been shown to have tremendous advantages in formation, heating, and of particular interest for propulsion applications, translation. The XOCOT project is focused on several unique properties and applications of FRC plasmas; the primary goal is to investigate FRC-based plasmas at low power (primarily lower voltages) and longer timescales, with specific interest in annular, coaxial FRC formation, optimization, and utilization. Similarly, investigations will focus on generating FRC plasmas efficiently, repeatably, and with large plasma densities.

Coaxial FRC Physics

Traditional FRCs have demonstrated high-velocity translation and high-efficiency compression. However, they also have some inherent disadvantages, namely high voltages (20-200 kV) and fast discharge times leading to complicated propellant feed and switching. A possible solution to these issues is the Coaxial Slow Source FRC concept (CSS) developed at the University of Washington by Vlases, Brooks, and Pierce for deuterium fusion[3,4]. This concept is based off of several annular, slow formation, AFRC concepts developed previously[5]. The CSS concept has demonstrated FRC formation and translation (in excess of 100 km/s with deuterium) at coil voltages of less than 100 volts and discharge times longer than 250 µs. The CSS has approximately 100-2000 V discharge voltages, 20-60 mTorr propellant pressures, and 100-500 µs discharge times. It successfully demonstrated results similar to traditional FRC concepts (LSX[6] etc.), however the temperatures were insufficient for fusion, and there was some evidence of the rotational n=2 instabilities that do not appear to be present in traditional FRCs. There was also evidence of excessive radiation losses due to the long discharge time and oxygen impurities. However, as our primary interest is FRC formation and immediate translation, these instabilities are of substantially less importance.

AFRL/UM XOCOT Concept

The AFRL/UM XOCOT[7] concept geometry is based upon the general geometry of the CSS device, but is scaled to incorporate lower discharge voltages. Upgrades in capacitor technologies, switching, and general device scaling have been done with the goal of re-tooling this general concept into one focused on lower voltages and internal diagnostics. Testing parameters are planned for 30-75 kA peak coil currents, 100-500 µs discharge times, over-all diameter of <40 cm, and >30 cm length. In addition, with argon propellant and a theta-ringing RF pre-ionization discharge the XOCOT is projected to have discharge voltages less than 1 kV. The current experimental validation concept consists of two quartz tubes forming the annular inner chamber, surrounded by two large discharge coils, with all components on a large stainless steel mounting/flange plate. The chamber is backfilled with argon, followed by the main coil discharge. Future designs will necessitate an annular region attached to a larger, non-backfilled vacuum chamber in order to fully characterize plasma translation velocities and performance specifics. Figure 1 is an artist's representation of the XOCOT concept.

AFRL FRC Technology Status Overview

The XOCOT facilities, energy storage, and switching networks have undergone significant upgrades in the last fiscal year to accommodate future research tasks. Additionally, operational regimes of energy parameters have been upgraded and expanded to facilitate the more complete exploration of pre-ionization and main bank discharges.
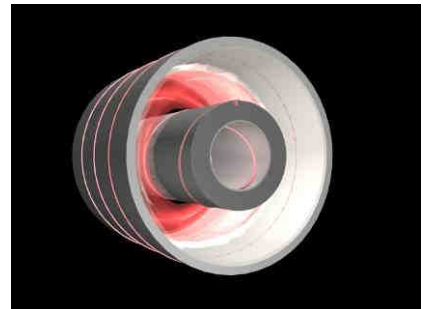

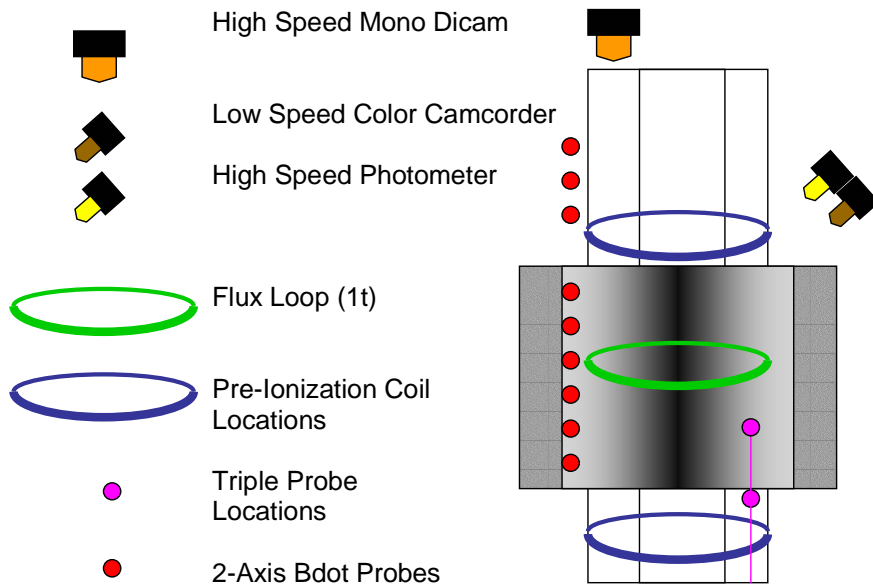Figure 1. 3D rendition of XOCOT Concept

3

Figure 2. Schematic of XOCOT diagnostic setup

XOCOT Facilities

- Two in-house manufactured aluminum coils (4 cm thick) are external to the chamber and form the theta coil assembly (Figure 3)

- Two 1.5 m long concentric quartz tubes which form the ionization region as well as the annular vacuum chamber (Figure 4)

- 20 cm diffusion pump and associated vacuum hardware

- 18 kJ,80 kA capacitor bank

- One 100 kA+ ignitron forms the main switching/transfer network

- High speed thyratron for pre-ionization Stage (Figure 4)

- Extensive physical, EMI, and UV shielding

- Associated high-energy safety mechanisms, including health monitoring, power dump, and bleed resistor systems.

Diagnostics (see Figure 2) **Error! Bookmark not defined.**

- Single-pixel high-speed photometer

- Highspeed Mega Pixel (MP) single frame camera

- Excluded flux array (36+ B-dot probes and several flux loops)

- Downstream magnetic field array

- Rogowski coil

- Internal double and triple-Langmuir probes

- Current and voltage monitors

Future hardware development will be targeted towards diagnostics including higher speed streak photography, holographic interferometry, spectroscopy, and bolometry.
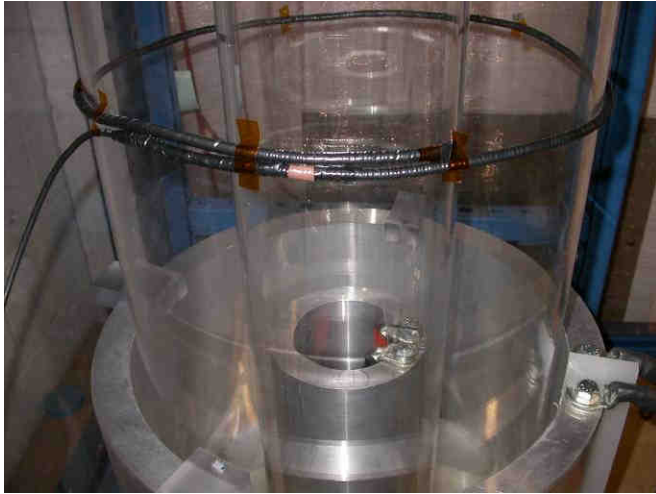

Figure 3. Photo of the inner and outer discharge coils mounted with the annular quartz vacuum chamber. Also shown is a 40 cm Rogowski-coil and high-frequency electro-magnetic shielding
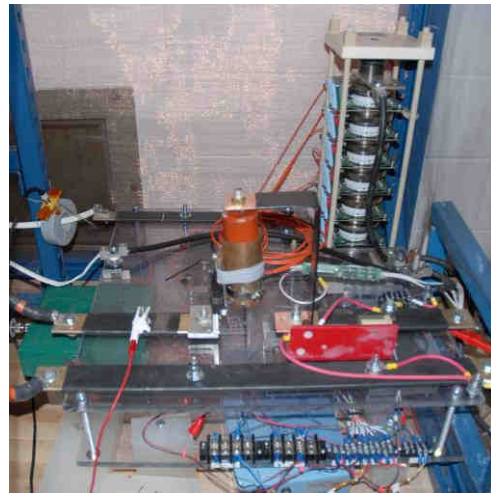

Figure 4. Switching Network. Shown are the high speed Thyristor switch and the high power ignitron main bank switch along with associated triggering and safety electronics.

The simplest diagnostic (and noiseless) that shows plasma formation and qualitative density changes is the single pixel photometer used to collect broad spectrum optical emission with a temporal sensitivity of >1Mhz. This diagnostic is a simple, general estimate of plasma formation and intensity, though its biggest liability is the lack of response in the lower wavelength regions typical of an ionized argon state, as shown in the spectral sensitivity data in Figure 5. Additionally, the photometer results are a complicated convolution of geometry, ion temperature, and plasma density, so while it does yield qualitative numbers for plasma intensity, care must be taken to fully explore plasma parameters.

Continuing with the optical diagnostics, a mega-pixel 3-color (RGB) DICAM Pro has been installed that is used to create real time plasma profiles of optically-emitted radiation. The DICAM Pro has a broad spectrum spectral sensitivity as shown in Figure 6 and is set to record either

- 5µs short period in order to explore individual FRC evolution

- 120µs single FRC discharge to get an averaged FRC profile.

- 120µs single Pre-ionization discharge to get an averaged profile of pre-ionizations

- 1ms total FRC formation to get an averaged profile of multiple FRC's for different operational conditions

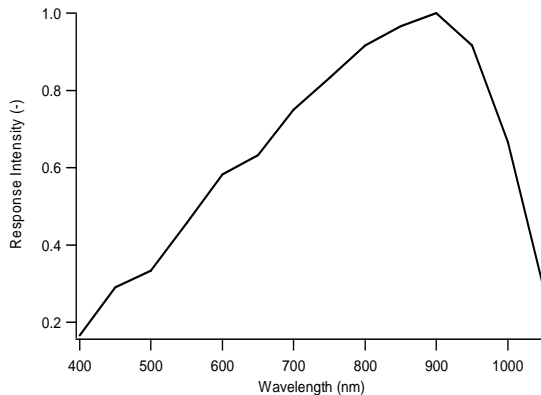This diagnostic is excellent for visualizing real time plasma formation and compression.

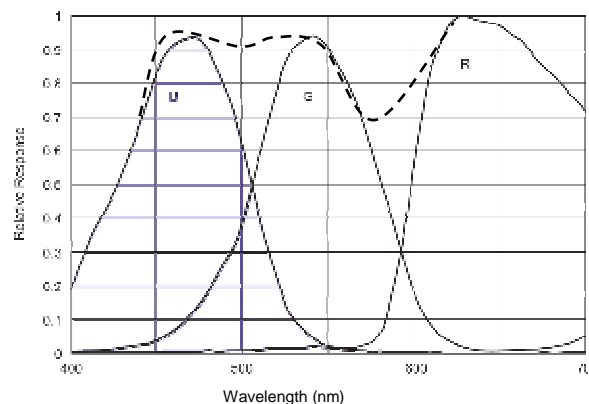Figure 5. Photometer spectral response data

Figure 6. Photometer spectral response data

5

Magnetic field probes are arrayed along the inner wall of the outer coil (see Figure 2), as well as downstream of the discharge coil. 'B-dot' probes follow Eqn 1 in order to calculate instantaneous magnetic fields within the XOCOT. They are digitally integrated after the data is collected at 10 MS-s.

$$V_{bp} = NA\frac{dB_p}{dt}$$ (1)

Similarly, an internal flux loop measures the rate of change of magnetic flux within the annular domain, and pairing these with the magnetic field probes yields an excluded flux array (EFA) to measure the plasma boundary of the FRC during compression and heating of the plasma as in Tuzewski[6]. Additionally, these magnetic field probes can qualitatively show the magnitude of compression and efficiency of magnetic coupling between the discharge coils and the magnetized plasma. This is also used to try and analyze the uniformity of the discharge and movement downstream. As shown in Figure 2 there is also a magnetic field probe 'rake' downstream of the discharge coils in order to track downstream magnetized plasma content. The primary measurement is axial magnetic field, the field that is generated by the main discharge, as well as the reversed current in the magnetized plasma. However, some azimuthal magnetic field data is shown, indicating more clearly (as the only azimuthal current generated is from the FRC) the timing, location, and strength of the magnetized plasma in the coil.

As shown in Figure 2, an internal triple Langmiur probe was placed inside of the annular region in order to calculate plasma parameters. For the pre-ionization discharge it was placed approximately 2cm below the axial location of the pre-ionization inductive coil. For the main discharge, the internal probe were positioned outside of the main magnetic field (to reduce magnetic gyro-radii and sheath modification effects on collected current). Both an internal triple Langmuir probe and double Langmuir probe were tested in the main bank discharges in order to use the more robust (but requiring multiple discharges for a single measurement) double probe to validate the individual triple probe results. The comparison is discussed later in the main bank discharge section of the paper.

Basic double probe theory[8] shows that a double Langmuir probe has two electrodes (in this case 0.55 mm diameter tungsten) that are biased with a fixed voltage between them. As that bias voltage is swept between two symmetric saturation regions (where both probes are either in ion/electron saturation regions) a plasma density and temperaturve relation are obtained (Eqn. 2). There are significant minimum conditions relating the probe size and relative positions that must be accounted for and have been specifically applied to the more dense plasma cases. This leads naturally to an error in the less dense plasma conditions, decreasing the measured density; these errors will be discussed further in a later section.

$$I = I_{sat}\tanh\left(\frac{V_\Delta}{2Te}\right)$$ (2)

Triple probe theory[9] is closely related to double Langmuir probe theory, with the addition of a single, high impedance floating probe (with no bias) that floats with the plasma; Additionally, the fixed differential voltage between the 'double probe' is set so that the probes are in a saturation regime. The triple probe is used to collect plasma temperature and electron density at various locations (see Figure 2).

Downstream, a unique collection of diagnostics is used to examine the plasma transport farther from the coil, while still utilizing entirely external diagnostics. Two time of flight (TOF) systems have been installed, the first, an excluded flux array, similar to the internal EFA measured real-time magnetic flux data to examine when (and for how long) the downstream diagnostic array senses magnetized plasma. Additionally, two collimated photometer detection systems have been installed that will, via fiber optic connections (to reduce E/M noise on the system), examine the passage of radiating plasma as it passes the two collimated probes. They are collimated to ~5 mm diameter, passed through a 0.5 mm fiber optic, and received into the photometer systems outlined above. By combining these two systems downstream plasma can be collected and examined non-invasively.

Pre-Ionization Experimental Results

As expected, pre-ionization of the FRC plasma, both in terms of the uniformity and total ionization fraction is a major factor in terms of the efficiency, symmetry, and repeatability, of an FRC formation. To that end, a significant portion of the current research focuses on pre-ionization techniques and characterization. It has been found that the large, low-voltage type FRC's that UM is producing require significant pre-ionization in order to yield high magnetic coupling to the plasma. Three major pre-ionization techniques have been studied. First, a single extra azimuthal coil that is given a 0.5-3kV MHz ringing discharge that should quickly (and indeed does within 3 oscillations), ionize the plasma within several skin depths. This discharge is driven by a 4 capacitor bank with 0.2uF capacitance, and 0.25 Mhz ringing frequency. This is the main pre-ionization technique and the various data from its operation are detailed later. The second and third ionization methods are a 'seed' ionization low power pre-ionization technique. The concept behind this is a low energy, unobtrusive ionization method that provides very little ionization fraction (and low plasma temperature) but provides a seed ionization for the ringing pre-ionization in order to hasten the plasma breakdown, lower breakdown voltages, increase ionization uniformity, and increase ionization spread. This is accomplished with:

- <150W RF 13.56 MHz discharge of a 3-turn inductive coil
- 2W DC Discharge with a thoriated tungsten electrode (1cm length) at pump-coil interface (see Figure 2)

This paper primarily deals with using a DC discharge as the seed ionization. Pre-ionization discharges less than 10 mTorr were done with RF, while discharges above 10 mTorr were done with DC seed ionization.

Figure 7 details the complete electrical circuit for the XOCOT testing being done. Included in this figure:

- DC charging supplies for both a pre-ionization capacitor bank and main, high power bank
- Ignitron switch for main bank
- Thyristor switch for pre-ionization bank
- Main and Pre-Ionization inductive coils
- Bleed resistors for main bank

This simplified figure does not encompass some of the implicit electrical details but is useful for the following discussions.
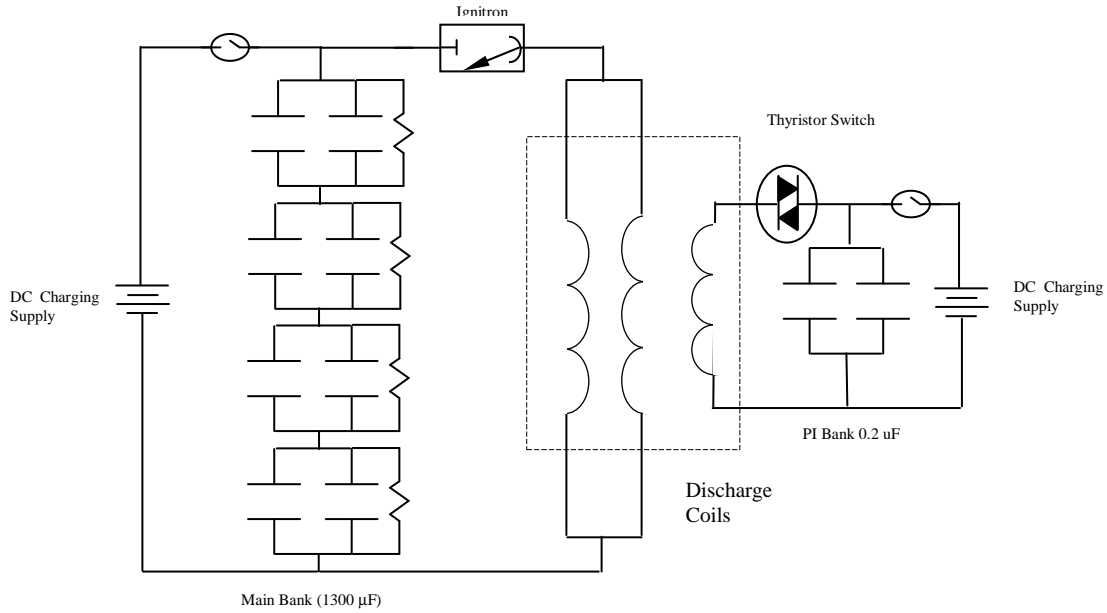
Figure 7. Electrical Diagram of main discharge circuit components for the XOCOT concept

Main Bank Discharge Experimental Results

   The same methodology of pressure, energy, and timing exploration has been performed for several main bank discharges. First a general description of discharge physics, electrical timing, and diagnostics is presented, followed by a detailed investigation of one typical discharge and, finally, a detailed investigation of trends in XOCOT discharges.

450 μs Discharge Period

   Figure 7 shows the general electrical circuitry and discharge hardware for the XOCOT discharges explored below. Figures 8 and 9 show data collected for a typical 450 ms discharge, in the detailed data, discharge voltage was 500V. Shown in Figure 8, the DC seed ionization is initiated 1 second before the main discharge. The pre-ionization discharge is triggered, and then 10 μs later (after the majority of the pre-ionization electrical noise has dissipated) the main bank is discharged. The pre-ionization discharge has a period of 2 μs, while the main bank has a period of 450 μs. Shown are the voltage and current of the inductive coil for a vacuum discharge (with a plasma there are differences in the induced plasma resistance and therefore voltage). It must be noted that actual bank voltages are higher than the coil voltages due to inductive losses in the switches and conductive paths. This is a minor effect for the main bank, but a major effect for the pre-ionization bank, where voltages on the capacitors may be 3-4 times as large as the voltages on the coil.
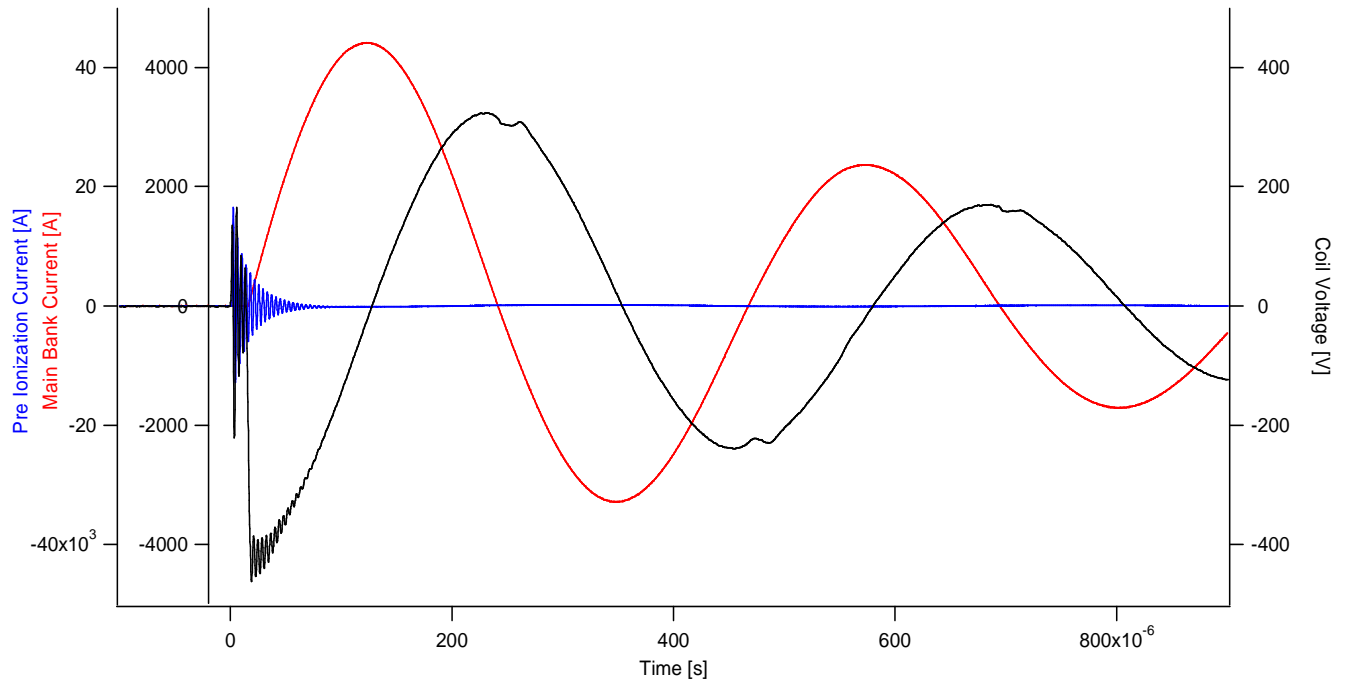
Figure 8. 500V Discharge showing total discharge current (both coils), pre-ionization current, and instantaneous coil voltage for a 250 μs discharge..
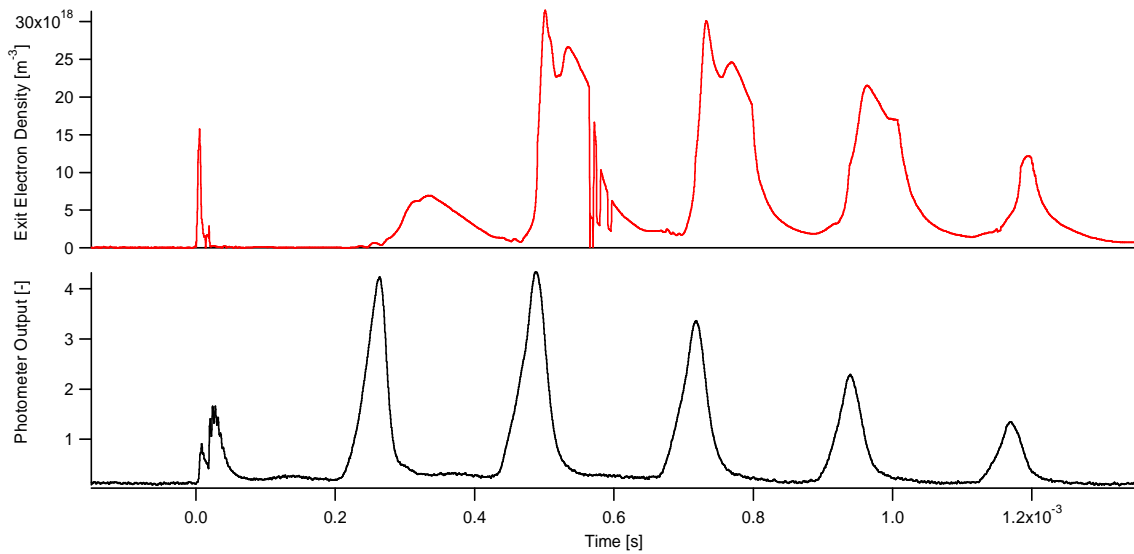

Figure 9. A 500V, 14 mTorr discharge showing multiple plasma formation and implosions. (a) shows electron density measured outside of the discharge coil, while (b) is direct instantaneous photometer results.

The three main diagnostics (of the many diagnostics in Figure 2) used in this analysis are an optical high speed mega-pixel DICAM, an array of magnetic field probes, and an internal triple probe located at

the edge of the main discharge coil (in order to minimize magnetic field error effects). With coil voltages greater than 200V and bank discharge periods less than 500 μs, very repeatable results have been achieved, showing multiple magnetized plasma formation and collapse with a single pre-ionization and main bank switching. Figure 9 shows plasma density measured at the coil edge and corresponding photometer results for a 500V, 14 mTorr discharge. Clearly, six plasma intensity increases and density pulses are evident in these charts, though they appear to vary widely in terms of magnitude and instantaneous profiles. These multiple pulse trends are typical and the first two peaks are very repeatable as shown later in Figure 15. At this stage it should be noted that the first plasma pulse is quite weak (both in terms of brightness and effluxed plasma), that the second pulse is much brighter than its corresponding effluxed density, and that similar structures exist in both density and photometer results between later pulses. These details will be explored more in later sections. The pre-ionization discharge is visible in the photometer results of Figure 9 in the first brightness peak during the 0-20 μs period at the beginning of the discharge.

Time	Mode
250-255 μs	Initial formation and reversal
260-265 μs	Radial compression and heating
270-275 μs	Radial compression / Rotational Instability
280-285 μs	Instability leading to radial expansion

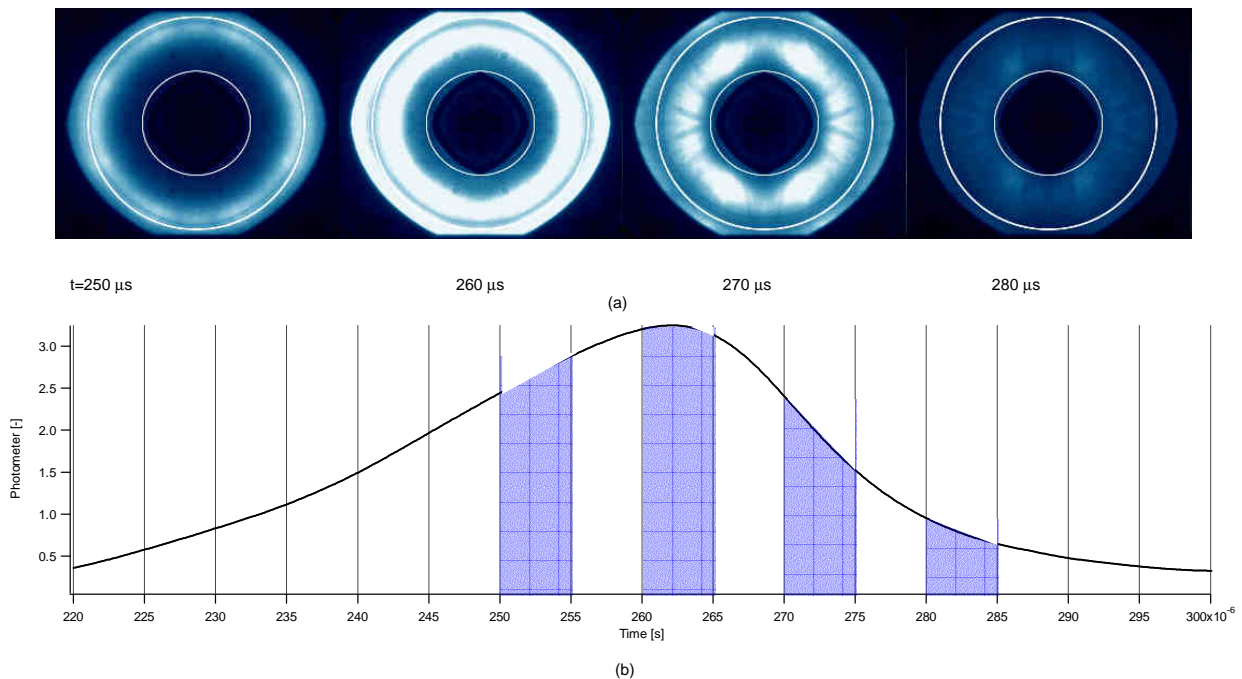Table 1. Typical formation and compression regimes

Figure 10. (a) Four 5μs integrated 1 MP photos of several 500V discharges.
(b) Photometer data with shaded timing indicating when high speed photographs taken.

Figures 10a,10b continue with the optical exploration of the evolution of these plasma pulses by detailing the formation (and collapse) of a pulse from 200 to 300 μs. Each photo is top-down with the same DICAM sensitivity settings (2.5 [-]) and a 5 μs integration/shutter time. The photos are taken during the four shaded areas of the photometer data (Figure 10b).   Similar analysis in past FRC experiments

have shown very similar results with four distinct formation/compression regimes present[6], as detailed in Table 1.

Figures 11 and 12 show preliminary results from the array of magnetic field probes between the discharge coil and the quartz chamber wall. Figure 11 shows the actual B-dot probe results (scaled to Gauss/sec) comparing a vacuum discharge (with no plasma or brightness changes) and a 20 mTorr discharge case that shows the magnitude of magnetic field change due to the magnetized plasma. This change is primarily due to the induced plasma current as the plasma toroid responds to the applied discharge current (and magnetic field) and shows clearly that high density magnetized plasmas are being formed inside the discharge region. Figure 12 are the digitally integrated results showing the change of magnetic field as compared to the applied magnetic field resulting from the discharge current. For these data the magnetic field (near the coil) is reduced by 5-10% depending on various discharge conditions. In Figures 11 and 12 data were taken at position 'AX1' which is 8 cm below the top of the main discharge coil (and pre-ionization discharge coil).
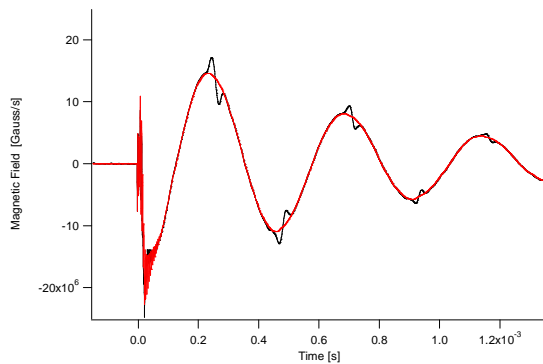
Figure 11. Magnetic field probe data for a vacuum and 20 mTorr discharge case with a coil voltage of 600V
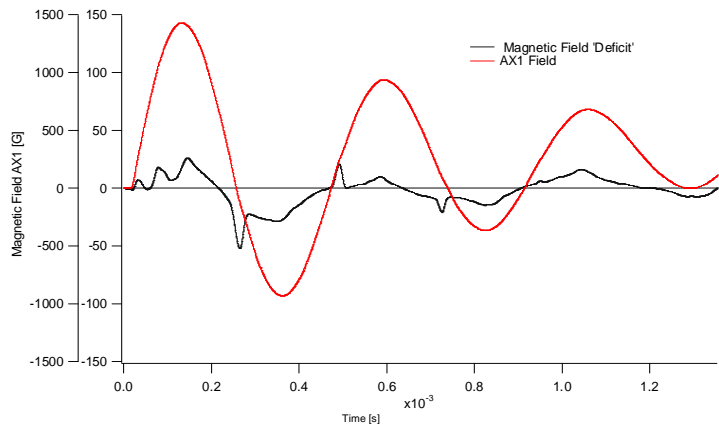
Figure 12. Magnetic field deficit for a 500V 14 mTorr discharge

Plasma density and temperature were measured 2 cm below the bottom edge of the coil (opposite the primary pre-ionization coil). As discussed above this triple probe consists of a biased double probe and a floating plasma potential probe. Multiple discharges were performed and the probe voltage swept in order to attempt to generate a composite set of double probe curves at all points in the discharge. The driving motivation for this process is electron temperature, which is elucidated in the slope of the linear region of Eqn 2. Plasma density is primarily dependent on collected current, gas properties, and probe area, and tends to be relatively low in relative error (between data sets for a given electrical setup and probe design). Clearly, this analysis requires the assumption that the discharges are highly repeatable and that the probes satisfy both double and triple probe requirements at all points in the discharge. These assumptions only appear to be valid during the first two discharge plasma pulses, and at the higher density conditions, therefore the double probe curves were only generated at these conditions. Figure 13 shows the multiple discharge I-V sweeps for a variety of discharge voltages. Figure 14 shows the triple probe calculated electron temperature (at a bias voltage of 36 V) compared to several double probe I-V curve calculations of electron temperature. The error bars shown in Figure 14 are the errors associated with the curve fit to the double probe data and are representative of error in the data of an individual voltage sweep, not overall relative error that is common to both double and triple Langmuir probes. The results are surprisingly good for the first 500 μs and at the peaks of later data points, with the average electron temperature being very similar; this trend continues across the entire range of data taken. There appears to be some lack of symmetry in the double probe sweeps (as shown by the +/- 46 V cases) that is typically due to asymmetries in the plasma on the scale of the double probe electrode separation distance. The triple/double probe result data were then collected at many operating conditions from 175 to 1000V and 8-30 mTorr; Figures 15-19 show the results of triple probe and photometer results for these tests.
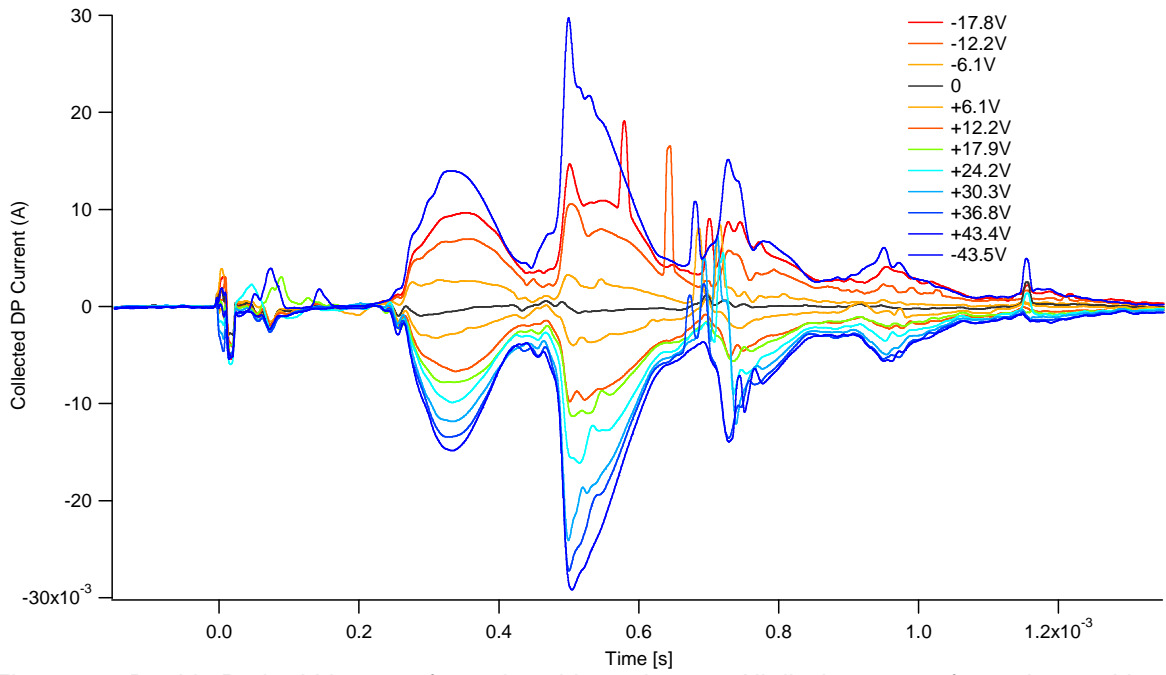
Figure 13. Double Probe I-V curves for various bias voltages. All discharges performed at 500V and 14 mTorr
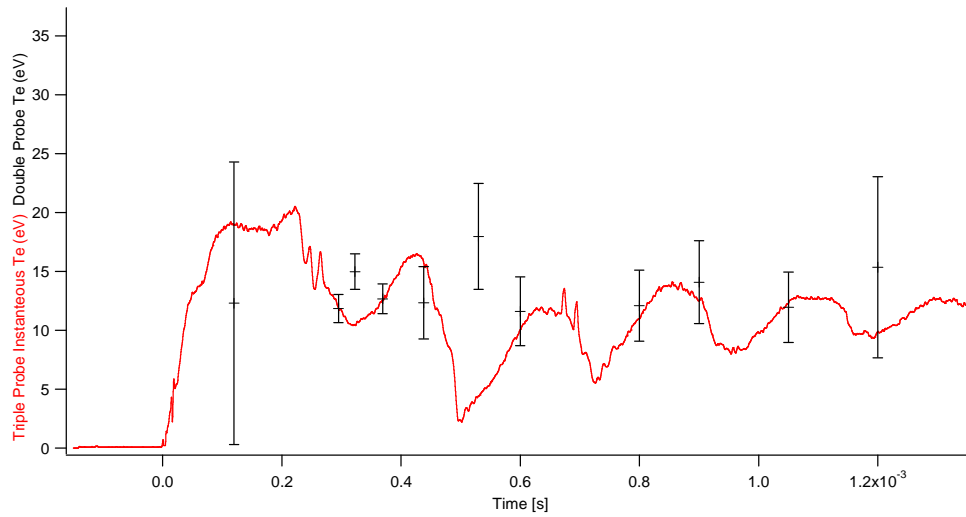

Figure 14. Comparison of triple probe Te to a congregate double probe temperature measurement at the highest confidence points.

Figure 16 details multiple background neutral densities and has clear trends; as pressure increases the density of each discharge increases as well as broadens. At the highest pressures the second and third major peaks have similar densities. Not shown here, at higher fill pressures, there exist more secondary peaks; 2 defined peaks at 8 mTorr to as many as 8 major plasma peaks at 30 mTorr fill pressure. For Figures 15 and 17, as expected, with increasing input energy (coil voltage and discharge current) the plasma densities increase, and the intermediate plasma densities stay higher.   It also appears that for successively higher powers the temporal peak in density (or when the plasma reaches the triple probe) is delayed , with the exception of the lower pressure, 700V cases. Why those cases appear to deviate from the trend of the rest of the discharges is still in question, for both the magnitude of the density peaks as well as the timing of the plasma reaching the triple probe. The two most important characteristics in Figure 15-17 is that the first peak is still quite weak and does not last for very long, and the second peak is much smaller than the subsequent discharges. This is not shown in the photometer results, which indicate that the second peak is much brighter, and for longer times, than any of the rest of the discharge pulses. This implies that the highest plasma content pulse is forming and compressing but not evacuating the chamber below the coil. Downstream data is necessary to confirm that indeed, the first major pulse is effluxing in the downstream axial direction.

Indeed, Figures 18 and 19 show well defined discharge pulses as evidenced by photometer data (including the first two). Also, trends that we would expect still are seen; with increasing power and/or neutral fill pressure, the discharge intensity (and the internal plasma density) increases as well as extending for many more pulses. Also, at the higher pressure cases there is more continuous plasma in the annular region.
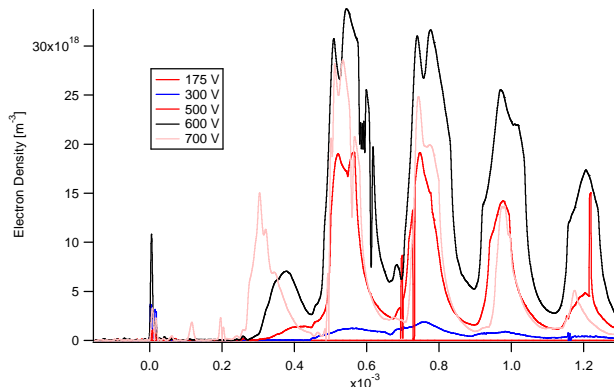

Figure 15. Downstream density for multiple discharge energies at 30 mTorr
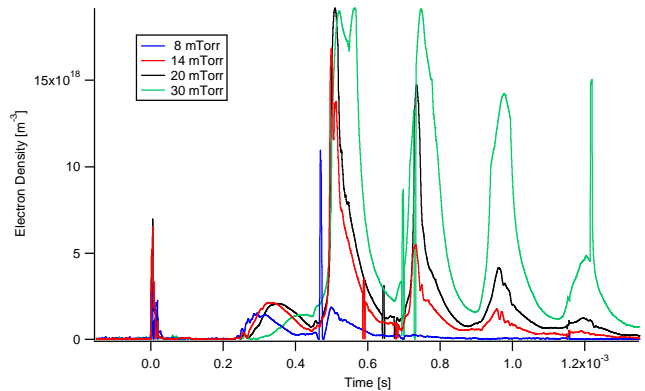

Figure 16. Downstream density for a 500V discharge at multiple background pressures.
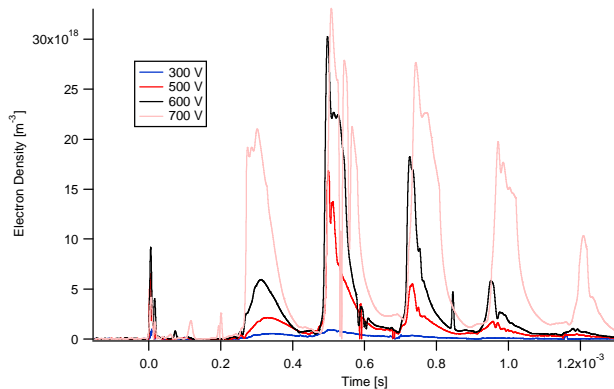

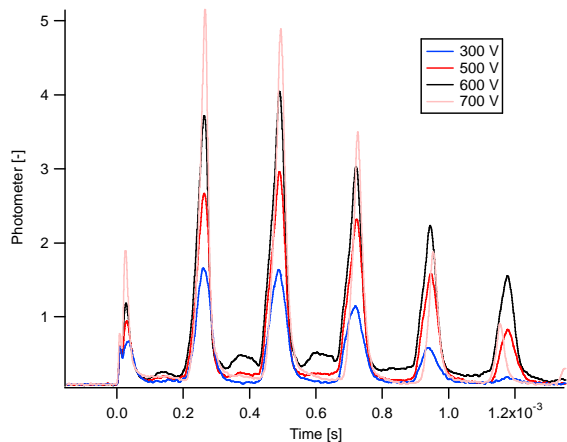Figure 17 Downstream density for multiple discharge energies at 14 mTorr

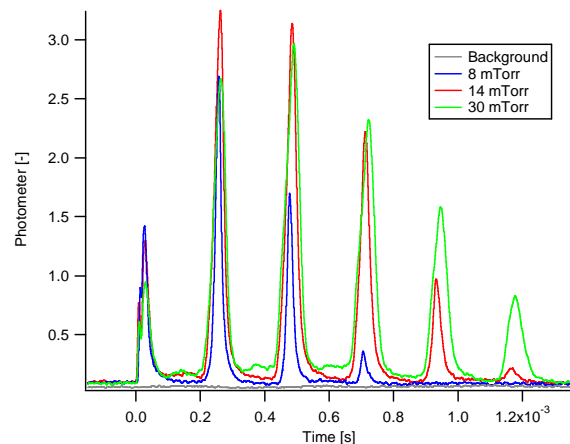Figure 18. Discharge photometer 'brightness' results for multiple discharge voltages at 14 mTorr

Figure 19. Discharge photometer 'brightness' results for multiple neutral fill pressures at a coil voltage of 500V

Figures 20 and 21 show these trends in a summarized format, as well as a direct comparison of peak plasma densities at various operating pressures and voltages. Figures 11-12 show magnetic field deficits measured (due to the magnetized plasma) for a single discharge. Figure 22 details the peak change in magnetic deficit, which can be looked at as the peak magnetic pressure, confinement, or compression of the magnetized plasma along the coil wall for various background fill pressures. From this, it appears that for the earlier plasma pulses the asymmetry in the heating and compression is rather large (>50% change in B-field) in the axial direction, with the most magnetized plasma near the pre-ionization discharge coil. For subsequent discharges (Figure 23) this is no longer the case, even though average magnetic field is also reduced. Finally, the trend to higher fill pressures continues, with significantly more magnetization, for longer periods at the same discharge energy at higher neutral densities.
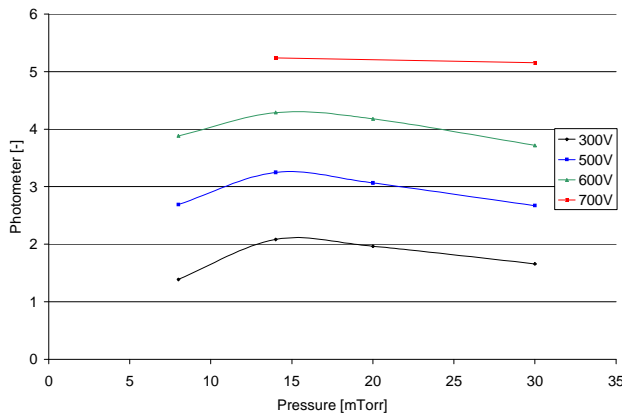

Figure 20. Peak photometer results as a function of background pressure for multiple discharge voltages. From 200-400 μs.
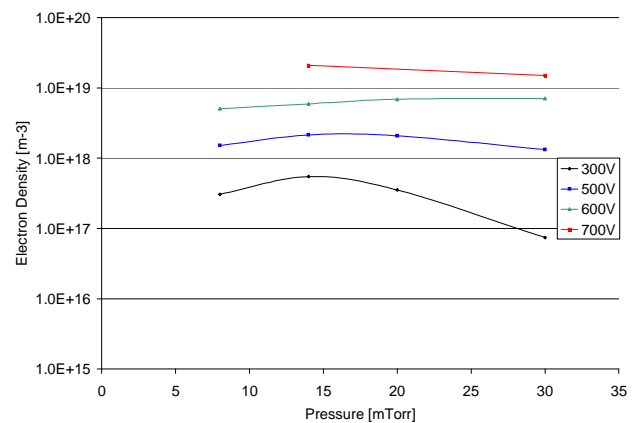

Figure 21. Peak Electron densities measured as a function of background pressure for multiple discharge voltages. From 200-400 μs.
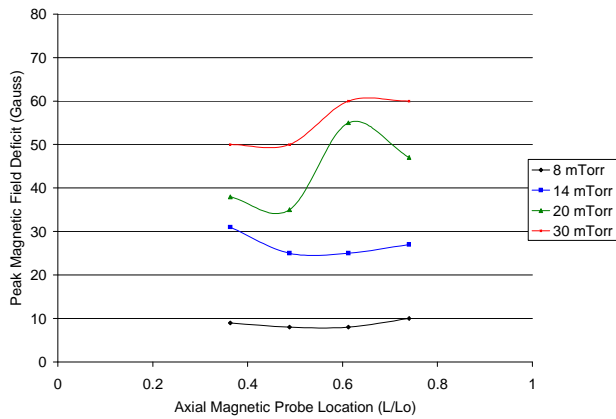
Figure 22. Peak magnetic field data for axial locations and various fill pressures. Discharge was 600 V, from 400-600 μs
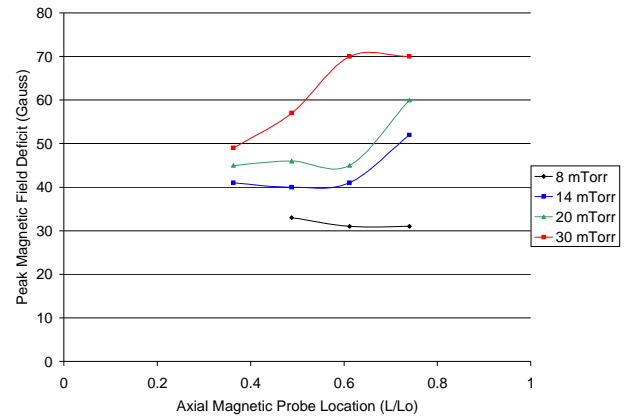

Figure 23. Peak magnetic field data for axial locations and various fill pressures. Discharge was 600 V, from 200-400 μs

250 μs Discharge Period

Similarly, experiments were performed for a shorter, higher dI/Dt, discharge with a period of 250 μs. Figures 24 and 25 shows the typical discharge pattern, though with an extended pre-ionization diffusion time that will be discussed later (the time between the pre-ionization pulse and the main discharge).
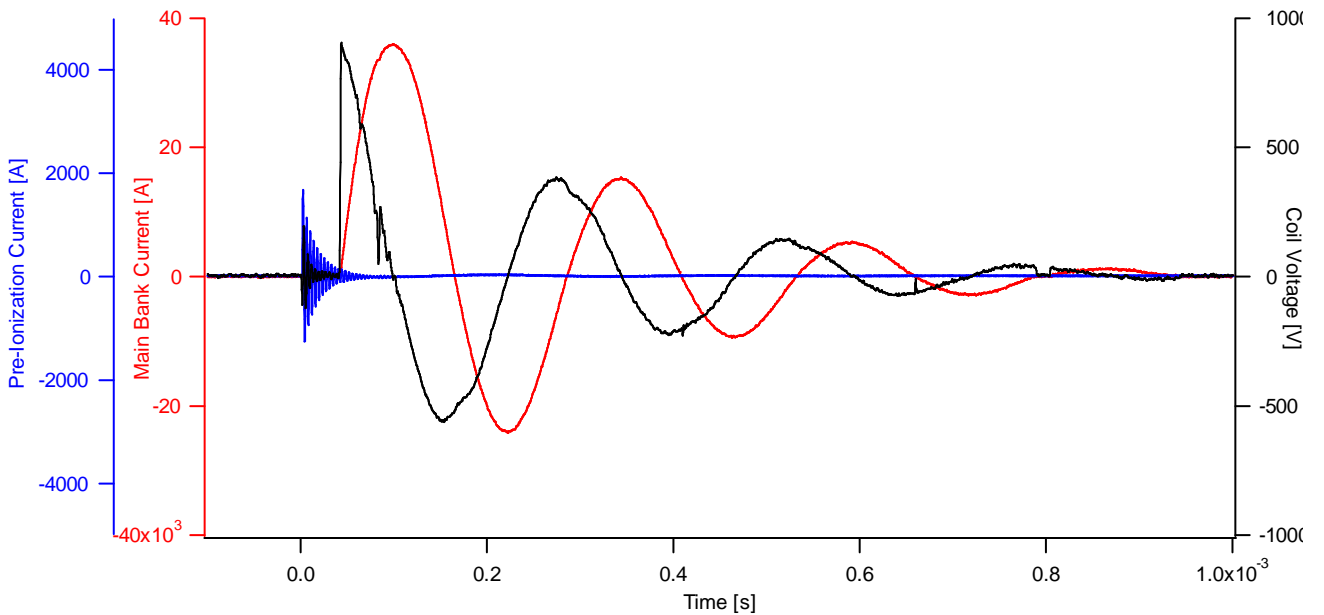

Figure 24. 750V Discharge showing total discharge current, pre-ionization current, and instantaneous coil voltage for a 250 μs discharge.
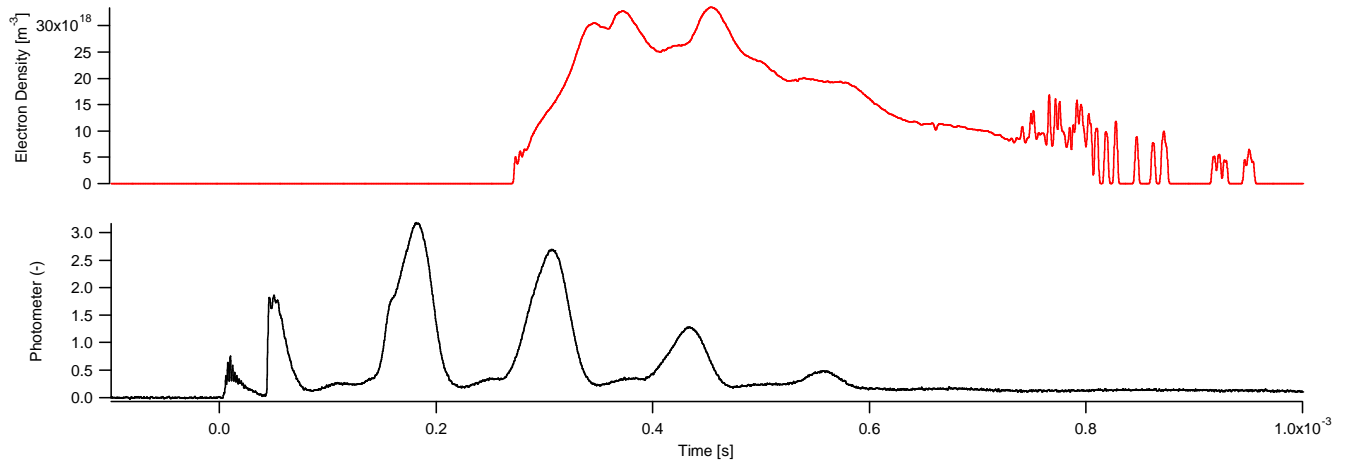
Figure 25. A 750V, 15 mTorr discharge showing multiple plasma formation and implosions. (a) shows electron density measured outside of the discharge coil, while (b) is direct instantaneous photometer results.

The photometer results are similar to the 450 µs case, but with some notable, and interesting differences, see Figure 25. The peak brightness from the FRC discharge is very repeatable, but less symmetric than from the longer discharge case, with a larger first ionization and wider, secondary ionization. Also, the dark zones interspacing the main re-ionization pulses are brighter and have a larger lead-in to the breakdowns that occur. Secondly, as shown in Figure 25, there is greater upstream plasma leakage density than in the 450 µs case, but it occurs at a much later time in the discharge. There is very little of the first two pulses upstream, and instead one large plasma mass that arrives a full 200 µs later than the initial discharge. As the triple probe data taken in these sweeps is unfortunately upstream, rather than downstream in the direction of a moving magetized plasma toroid, this actually implies that we have little backstreaming plasma and that the measured data is either slow diffusion after compression (and ejection) or, less likely, reflected higher energy plasma. Further tests must be done to differentiate the results.

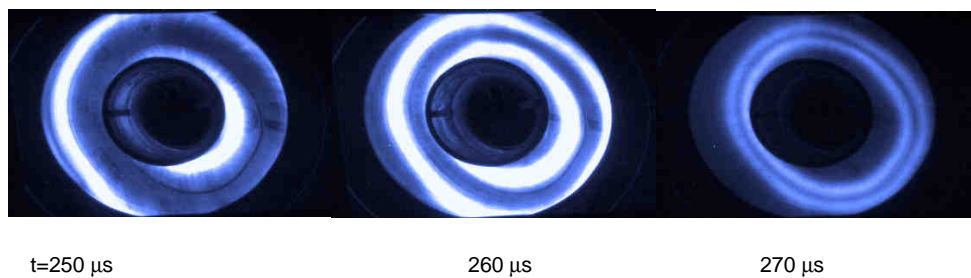t=250 µs   260 µs   270 µs

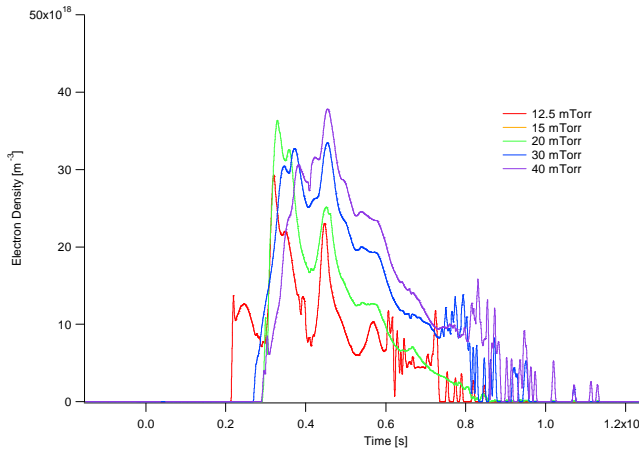Figure 26. Downstream Photography

Figure 27. Downstream density for multiple neutral pressures for a 750V discharge case.

Figure 27 shows upstream plasma results for multiple discharge neutral fill densities. As expected, fast results mirror the slower discharge results in that increased discharge energy and increasing background pressure increase plasma brightness and density of formation for the upstream plasma.

Figure 28 shows raw B-dot probe results for multiple pressure discharges. This is explored further in Figure 30, however, qualitative results can be garnered by examining the timing and relative magnitude of magnetic field effects. Clearly, there are significant effects compared to the vacuum discharge case (black), even more significantly there appears to be an increased (though apparently initiated later) magnetic deficit due to the larger background pressure cases. This effect becomes more pronounced for the later reversals. Also, we can see that the magnetized plasma starts to become apparent (on the scale of the main discharge (10's of Gauss) approximately 10 µs before the field zero (10 µs before the largest dI/DT) and continues for 75 µs beyond it.

For the 250 µs discharge testing a unique analysis was done in order to study the effect of the non-
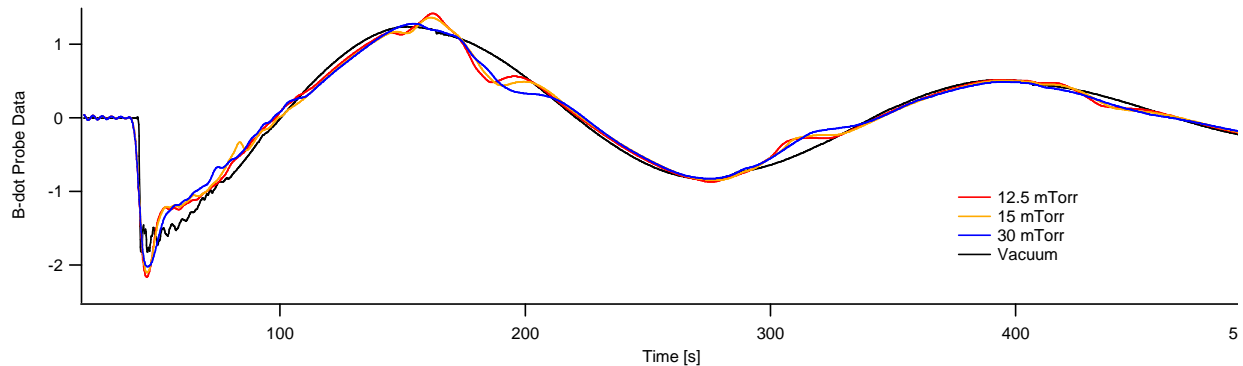

Figure 28. B-dot probe results for 750V discharge case for various input pressures to examine plasma compression as a function of input neutral density.

uniformity in the pre-ionization discharge that was discovered in the previous 450 µs testing. The delay time between the pre-ionization discharge initiation and the main flux addition discharge was varied between 0 and 50 µs. The goal of this examination was to allow the pre-ionization plasma to disperse more evenly throughout the annular discharge region between beginning the main flux addition and reversal. Expected was a peak plasma formation; as the plasma disperses it also decays thereby setting a unique maxima in peak brightness and plasma content. Shown in Figure 29, the peak plasma formation is between 40 and 50 µs of delay time as detailed by the broad band photometer results.
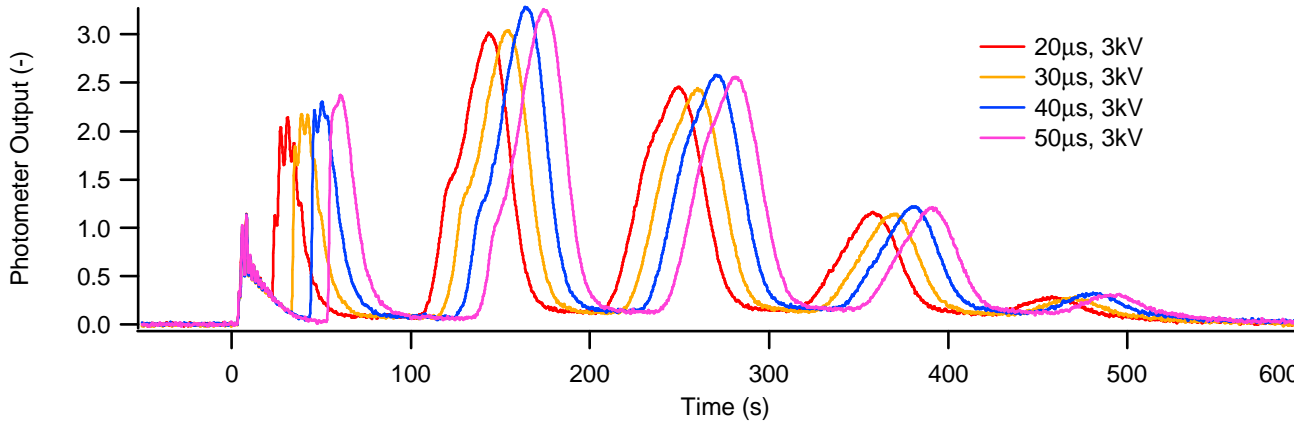
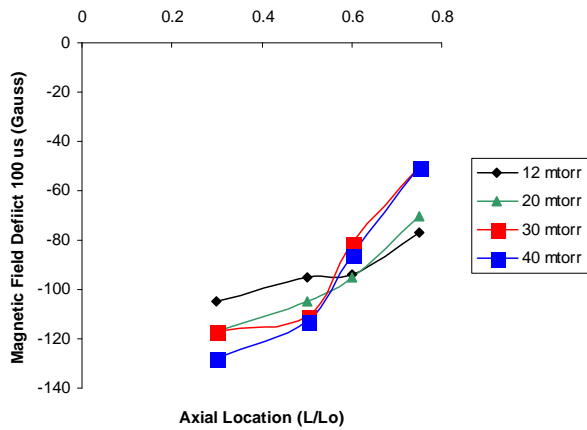Figure 29. Photometer results for multiple pre-ionization timings.

Figure 30. Peak magnetic field data for axial locations and various fill pressures. Discharge was 750 V
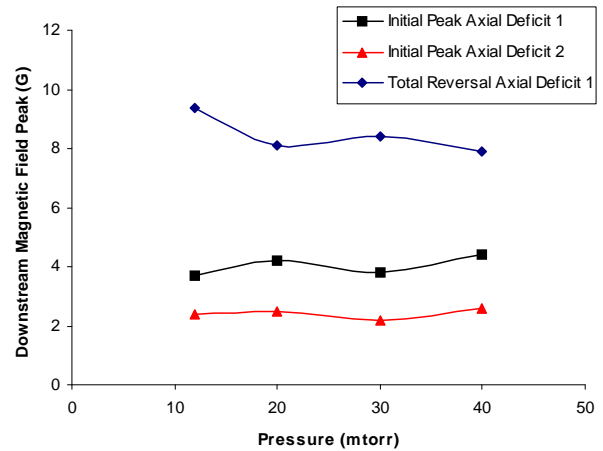

Figure 31. Downstream magnetic field peak and reversal as a function of pressure.

Figures 30, 31 continue the investigation into magnetic field effects. Figure 30 shows the magnetic field deficit (as compared to Figure 22 for the 450 μs discharge case) shows similar trends as before, with higher neutral pressures yielding larger magnetic field shielding and also stronger non-uniformities related to the pre-ionization distributions. Surprisingly, the magnitude of the deficit is 200-300% larger than with the 450 μs case. This effect is due to the larger dI/Dt and induced fields in the plasma. Figure 31 shows some of the downstream effects from the magnetic field probes placed 0.8 m downstream from the exit of the discharge coil, external to the vacuum annulus. They show ~ 9 Gauss field reversal at 0.8 m downstream with approximately 35% decrease in magnetic field 0.15 m farther downstream. This is either a function of decrease plasma density (and magnetization) due to plasma interaction with the background neutral gas or a decrease in separatrix radius as the plasma proceeds downstream. To understand the differences, and gain more understanding of the detailed mechanisms of downstream travel, internal magnetic and plasma probes must be placed within the FRC travel path, which was unavailable for this experimental setup. Further setups will seek to clarify and detail this information.

Summary

A field reversed configuration (FRC) plasma generator concept has been developed at AFRL by the University of Michigan. Presented, has been research into examining and optimizing the creation of magnetized FRC discharges. Specifically, it has been shown that sucessful pre-ionization and main bank discharges have lead to the creation of multiple high-density magnetized plasma pulses per main bank discharge. This paper has investigated a range of pressure, discharge energy, pre-ionization settings, and discharge timings and their effect on plasma production. However, while it has been quite clear that formation of the latter of these high density, magnetized plasmas is repeatable and effective, there are clear problems with the first expected field reversal and plasma pulse, leading to the general conclusion that pre-ionization is not yet geometrically uniform enough to form FRC's on the first discharge oscillation and require further heating (in this case from the main bank) to be sufficient. Additionally, the high speed triple probe as a diagnostic in this type of discharge regime has been explored and further validated as a suitable diagnostic for plasma parameters, though further work will be focused on probe location and how this affects plasma results. This experimental analysis has suggested further improvements and discharge paramters to focus on, namely higher neutral fill densities, coil voltages greater than 500 V, and a more distributed pre-ionization electrode design.

References

[1] Kolb, A.C., Dobbie, C.B., Phys. Rev. Lett. 3, 5 (1959).

[2] Steinhauer, Loren C., "Recent Advances in FRC Physics", IEEE 0-7803-2969-4 (1995).

[3] W.F. Pierce, R.J. Maqueda et al, Nucl. Fusion 33, 117 (1993).

[4] Raman, R., Vlases, G.C., Jarboe, T.R., Nuclear Fusion 33, 1685 (1993).

[5] Jarboe, T.R. et al. Slow Formation and Sustainment of Spheromaks by a Coaxial Magnetized Plasma Source. Phys. Rev. Letters 51(1) (1983).

[6] M. Tuszewski, Nuclear Fusion 28, 2033 (1988).

[7] Kirtley, D., et al. "Details on an Annular Field Reversed Configuration Plasma Device for Spacecraft Propulsion", IEPC 2005, Princeton, NJ IEPC-2005-171

[8] Lieberman, M., Lichtenberg, A., "Principles of Plasma Discharges and Materials Processing". 1st Edition. Wiley, 1994

[9] Jen-Shih, C., et al., "The instantaneous triple-probe method for the direct display of plasma parameters in a low density continuum plasma". Journal of Physics D (Applied Physics), 1980. **13**(6): p. 1083.